The Effect of Flow Development Region and Fringing Magnetic Force Field on Annular Split-flow Thin Fractionation

Yonghao Zhang[*] *and David R. Emerson*

The Centre for Microfluidics, CLRC Daresbury Laboratory, Warrington WA4 4AD, UK

ABSTARCT: Split-flow thin (SPLITT) fractionation devices have been widely used to separate macromolecules, colloids, cells and particles. Recently, the quadrupole magnetic flow sorter (QMS) has been reported in the literature as another family of SPLITT fractionation device. However, the separation performance observed in the experimental measurements is generally found to deviate from the ideal behaviour. Possible causes such as hydrodynamic lift force, high particle concentration and imperfect geometries have been extensively examined. However, the effects of flow development regions and fringing magnetic force field at the separation channel inlet and outlet, which are ignored by the theory, have not been investigated. The error introduced by ignoring these effects need to be rigorously studied so that the theory can be used to optimise operation flow rates with confidence. Indeed, we find in this paper that these ignored effects are responsible to the discrepancy between the experimental data and the theoretical predictions. A new theory has been proposed for optimisation of device operation.

Keywords: Split-flow thin fractionation; CFD; Particle separation; Fringing magnetic field

[*] Phone: 44-1925-603149; Fax: 44-1925-603634; Email: Y.Zhang@dl.ac.uk

INTRODUCTION

Recently, the quadrupole magnetic flow sorter, which is a form of SPLITT fractionation device, has been developed to separate magnetic-bead-labelled cells [1-3]. A schematic diagram of this device is shown in figure 1. The sample enters the separation channel through the inlet *a* with a volume flow rate Q_a^{in}, the separated particles will be collected at the outlet *b*, where the flow rate is Q_b^{out}. Williams et al. [4] have established a theory for optimisation of operational flow rates. However, a consistent discrepancy has been observed between the theoretic predictions and the experimental measurements [2, 3, 5]. Williams et al. [6] have reviewed and studied the causes of the discrepancy. For an annular separation channel, the side-wall effect is absent, which removes a major concern as it is for a parallel-plate SPLITT device [4, 6, 7]. The other concerns such as lift forces and high particle concentrations have been investigated and their effects can be restricted [6, 8, 13]. Williams et al. [6] examined the effect of geometry imperfections and concluded that they play a significant role in the loss of resolution.

However, the current theory of Williams et al. [4] was established upon ignoring the effects of flow development regions and fringing magnetic force fields at the separation channel inlet and outlet. Here the separation channel refers to the part of channel between two splitters. As our previous work has reported [14], ignoring flow development region for a plane SPLITT fractionation device under a uniform force field may be acceptable, however, a significant error may be introduced for an annular SPLITT fractionation device. Moreover, the force field is no longer uniform and a fringing magnetic force field exists at the regions near the splitters, which may have considerable influence over the theoretic predictions. These effects, which may be the major causes of the discrepancies between the experimental data and the theoretic predictions, need to be examined. In this paper, analyses of these effects will be performed theoretically and numerically.

THEORY

Here, the annular SPLITT channel is assumed perfectly assembled so that the possible effect of geometry imperfections can be ruled out. The particle concentration is low and the inter-particle interactions are weak, thus the particle will not affect the fluid flow field. The only differences to the theory developed by Williams et al. [4] are that the flow development regions and the fringing magnetic force fields at the separation channel inlet and outlet will be addressed in the following theory.

The similar approach described in our previous paper [14] can be adopted except that a cylindrical coordinate is used here. Any laminar flow field in an annular channel can be described by the stream-line function $\psi(z, r)$:

$$V_z = \frac{1}{r}\frac{\partial \psi}{\partial r};\ \ V_r = -\frac{1}{r}\frac{\partial \psi}{\partial z}, \tag{1}$$

where V_z and V_r are the velocity components of the fluid in the axial and radial directions, z and r respectively. These streamlines are axi-symmetric, a corresponding stream-plane will be formed by rotating the stream-line against the axis. The volume flow rate between two stream-planes is given by:

$$Q_{1-2} = 2\pi\left[\psi(z_2, r_2) - \psi(z_1, r_1)\right], \tag{2}$$

where $Q_{1\text{-}2}$ is the volume flow rate between stream-planes 1 and 2.

Because the flow is not fully-developed at the separation channel inlet and outlet, the stream-planes are not parallel as previously assumed, the particle velocity at any point becomes,

$$U_r(z,r) = U_{mr}(z,r) + V_r(z,r); \qquad U_z(z,r) = V_z(z,r) + U_{mz}(z,r), \tag{3}$$

where U_{mr} and U_{mz} are the relative velocities between the particle and the surrounding fluid in the radial and axial directions. The existence of U_{mz} is due to the fringing magnetic force field. Not only do these relative velocities depend on the radial position, r, but also they depend on the axial position, z. By following the same procedure as given in Zhang et al [14], we reach

$$\frac{\partial \psi}{\partial r} dr + \frac{\partial \psi}{\partial z} dz = U_{mr} r dz - U_{mz} r dr . \quad (4)$$

Integrate from one arbitrary stream-line 1 to stream-line 2,

$$Q_{1-2} = 2\pi \int_1^2 (U_{mr} r dz - U_{mz} r dr) . \quad (5)$$

The operation flow rates can be related to the migration velocity by equation (5). For a parallel-plane SPLITT fractionation device under a uniform force field such as gravity, the right hand of equation (5) is a constant. Consequently, a simple relation between the critical flow rates and the particle migration velocity can be achieved [14, 15]. Unfortunately, the force field here is no longer uniform and the integral is particle trajectory dependent. Therefore, we need to determine the force field and the particle trajectory in order to solve equation (5).

MAGNETIC FORCE FIELD

Generally, a particle moving within a carrier fluid will experience forces from the fluid phase such as the drag force, the lift force etc. In addition, the Kelvin force due to the magnetic force field will also act on the particle. If these forces are assumed to be linearly additive (for better illustration purpose), the symbolic expression for the total forces, $\boldsymbol{F}$, can be given by

$$\sum \boldsymbol{F} = \boldsymbol{F}_{drag} + \boldsymbol{F}_m + \boldsymbol{F}_{added} + \boldsymbol{F}_{Basset} + \boldsymbol{F}_{Saffman} + \boldsymbol{F}_{Magnus} + \boldsymbol{F}_g + \boldsymbol{F}_b \ldots , \quad (6)$$

where, $\boldsymbol{F}_{drag}$ is the drag force; $\boldsymbol{F}_m$ is the Kelvin force; $\boldsymbol{F}_{added}$ is the added mass; $\boldsymbol{F}_{Basset}$ is the Basset force, $\boldsymbol{F}_{Saffman}$ is the Saffman force, a lift force due to fluid velocity gradient; $\boldsymbol{F}_{Magnus}$ is the Magnus force, a lift force due to particle rotation; $\boldsymbol{F}_g$ is the gravity force; $\boldsymbol{F}_b$ is the buoyancy force. Inter-particle hydrodynamic interaction is neglected as we assume a low particle concentration. Therefore, the dominate lubrication force at small distance between pairs of particles is not considered here. Because the quadrupole magnetic flow sorter is operated with its axis z in the gravity direction, the gravity force can be negated by the buoyancy force if the density difference between the particles

and the fluid is small. Here, the particle size is large enough that Brownian motion can be neglected and small enough that the relaxation time of the particle to the flow field is very small compared to the characteristic time scale of the flow field [14]. Therefore, the particle diameter needs to be greater than 1 μm [16] and have a Stokes number far less than unity [17]. As a result, the added mass, the Basset force, the Saffman force and the Magnus force are negligibly small in comparison to the drag force [14, 18, 19]. Therefore, we only need to consider the drag force and the Kelvin force here.

For a Stokes flow, the drag force is $3\pi\mu d\boldsymbol{U}_m$. For a particle with magnetic permeability μ_m freely suspended in an external magnetic field $\boldsymbol{H}$, the Kelvin force is given by [20]

$$\boldsymbol{F}_m = \frac{1}{2}\nabla(\boldsymbol{B}^2/\mu_m). \tag{7}$$

The external magnetic field $\boldsymbol{H}$ is related to the magnetic flux density $\boldsymbol{B}$ as $\boldsymbol{H}=\boldsymbol{B}/\mu_m$, where the magnetic flux density $\boldsymbol{B}$ can be determined by [20]

$$\nabla \cdot \boldsymbol{B} = 0. \tag{8}$$

Also from Maxwell field equations [20], we have

$$\nabla \times \boldsymbol{B} = \mu_0(\boldsymbol{j} + \varepsilon_0 \frac{\partial \boldsymbol{E}}{\partial t}), \tag{9}$$

where $\boldsymbol{E}$ is the electric intensity, $\boldsymbol{j}$ is the current density, ε_0 is a constant and μ_0 is the magnetic permeability of the vacuum. Within the separation channel, the magnet field is stationary and there is no current inside, so that the right hand of equation (9) is zero. In the experiments, the magnitude of $\boldsymbol{B}$ was measured at the quadrupole magnet tip which can be served as the boundary conditions for determining the magnetic force field within the separation channel. In doing so, we can avoid solving the complex quadrupole magnetic field outside of the separation channel. From equations (8, 9), the magnetic force field within the channel can be further simplified to be described by the following equation:

$$\nabla^2 \boldsymbol{B}^2 = 0 . \tag{10}$$

Here, we can introduce "magnetophoretic mobility", a term proposed in the literature [2-4]. Then, the particle migration velocity in an aqueous media under a magnetic field can be given by

$$\boldsymbol{U}_m = m_m \boldsymbol{S}_m , \tag{11}$$

where m_m is the particle magnetophoretic mobility, and the local force field strength $\boldsymbol{S}_m$ is given by

$$\boldsymbol{S}_m = \nabla\left(\frac{\boldsymbol{B}^2}{2\mu_0}\right). \tag{12}$$

The particle magnetophoretic mobility can be measured by a device called a CTV [2]. From equations (11, 12), we can see the particle migration velocity and the local force field strength can be determined once we solve equation (10). S_{mr} and S_{mz}, which are the magnetic force field strength in the r and x directions respectively, are given by

$$S_{mr} = \frac{\partial}{\partial r}\left(\frac{\boldsymbol{B}^2}{2\mu_0}\right) \text{ and } S_{mz} = \frac{\partial}{\partial z}\left(\frac{\boldsymbol{B}^2}{2\mu_0}\right). \tag{13}$$

FLOW FIELD

The flow field can be described by Navier-Stokes equations:

Continuity equation: $$\frac{\partial \rho_f}{\partial t} + \nabla \cdot (\rho \boldsymbol{V}) = 0 , \tag{14}$$

Momentum equation: $$\rho_f \frac{D\boldsymbol{V}}{Dt} = -\nabla p + \mu \nabla^2 \boldsymbol{V} + \rho \boldsymbol{g} , \tag{15}$$

where $\boldsymbol{g}$ is the gravity and ρ_f is the fluid density. Since one-way coupling is assumed, i.e. particles have negligible effect on the flow field, the Navier-Stokes equations are independently solved for the steady fluid flow in the channel. The classical SIMPLE algorithms have been well developed to solve Navier-Stokes equations. Many commercially-available solvers can be used to solve these equations. In this paper, we have used our own flow solver- μ-Thor 2.0 and the flow solver of CFD-

ACE [21], both give exactly the same answers for the creeping flows considered in this paper. The details of the employed SIMPLE algorithms are widely available, e.g. Ferziger and Perić [22].

CRITICAL MAGNETOPHORETIC MOBILITIES

The critical magnetophoretic mobility, m_0, for a particle trajectory that starts from the bottom of the splitter at the inlet *a* and ends at the splitter at the outlet *b* is

$$m_0 = \frac{Q_a^{out} - Q_a^{in}}{2\pi \int_{SI}^{SO} r(S_{mr} dz - S_{mz} dr)}, \tag{16}$$

where *SI* and *SO* refer to the positions of the inlet and outlet splitters. If the particles have a mobility smaller than m_0, they will all move out through the outlet *a*. The critical velocity, m_1, for a particle starting at the wall of the inlet *a* and ending at the splitter of the outlet *b* is

$$m_1 = \frac{Q_a^{out}}{2\pi \int_{WI}^{SO} r(S_{mr} dz - S_{mz} dr)}, \tag{17}$$

where *WI* refers to the position of the inlet wall. Particles with mobility larger than m_1 will all move across to the outlet *b*. In the case of separating fragile cells or if we want to reduce the number of particles sticking to the wall and increase the particle retrieval rate, another critical mobility is important, m_2, viz.

$$m_2 = \frac{Q_b^{in}}{2\pi \int_{SI}^{WO} r(S_{mr} dz - S_{mz} dr)}, \tag{18}$$

where *WO* refers to the position of the outlet wall. Under this critical mobility, a particle starting from the inlet splitter can just reach the outlet wall, so that any particle with smaller migration velocity from the inlet *a* will not hit the outlet wall. These three critical mobilities are essential for optimisation of operation flow rates. To separate two types of particles with mobilities of m_{m1} and m_{m2}, the operation flow rates need to satisfy the following criteria: $m_{m1} < m_0$, so that all the cells

with magnetophoretic mobility of m_{m1} will be collected at the outlet *a*; $m_1 < m_{m2} < m_2$, so that all the cells with magnetophoretic mobility of m_{m2} will move out of the outlet *b* without sticking to the wall.

If we ignore the flow development regions and the fringing force field at the separation channel inlet and outlet, the present theory as described by equations (16-18) can be simplified to the same as the theory developed by Williams et al. [4]. The advantage of the theory of Williams et al. is that it reduces computational effort significantly because there are analytical solutions for the velocity field and the force field. The velocity field in the annulus is fully-developed and it can be theoretically determined by

$$V_r = \frac{2\langle v \rangle}{A_1}(1 - \rho^2 + A_2 \ln \rho), \tag{19}$$

where <*v*> is the mean fluid velocity and $\rho = r/r_o$ (r_o is the radius of the outer wall of the separation channel as shown in figure 1). A1 and A2 are given by

$$A_1 = 1 + \rho_i^2 - A_2, \tag{20}$$

$$A_2 = \left(1 - \rho_i^2\right) / \ln\left(1/\rho_i\right), \tag{21}$$

where $\rho_i = r_i/r_o$ (r_i is the radius of the inner wall of the separation channel as shown in figure 1). Therefore, solving complex Navier-Stokes equations can be avoided. Moreover, by ignoring the fringing magnetic force field, S_m in the *z* direction can be assumed to be zero, and S_m in the *r* direction can be theoretically determined by

$$S_{mr} = \frac{B_o^2}{\mu_0 r_o}\rho. \tag{22}$$

Substitute equations (19, 22) into equations (16-18), and assume the particle entry radial positions to be the corresponding streamlines at fully-developed region, we can then obtain analytical solutions for the critical mobilities the same as given by Williams et al.[4]:

$$m_0 = \frac{Q}{2\pi r_0 L S_{m0}} \frac{I_1\left[\rho_{ISS}, \rho_{OSS}\right]}{A_1\left(1 - \rho_i^2\right)}, \tag{23}$$

$$m_1 = \frac{Q}{2\pi r_0 L S_{m0}} \frac{I_1[\rho_i, \rho_{OSS}]}{A_1\left(1-\rho_i^2\right)}, \tag{24}$$

$$m_2 = \frac{Q}{2\pi r_0 L S_{m0}} \frac{I_1[\rho_{ISS}, 1]}{A_1\left(1-\rho_i^2\right)}, \tag{25}$$

where

$$I_1[\rho_1, \rho] = \left[4\ln\rho - 2\rho^2 + 2A_2(\ln\rho)^2\right]_{\rho_1}^{\rho}. \tag{26}$$

NUMERICAL ALGORITHM

Hoyos et al. [2] produced the comprehensive experimental data, where they set $Q_a^{in}/Q = 0.1$ and $Q_a^{out}/Q = 0.2$ with a series of total flow rate Q. From these given flow rates and the measured magnetic flux density at the tip of the quadrupole magnet B_0, we can determine the critical magnetophoretic mobilities by solving equations (16-18). However, the integrals are carried out along the particle trajectories, but the particle trajectory also relies on the value of the mobility, numerical iterations are needed to solve this coupled phenomenon.

Because we have assumed that the flow field and the magnetic field are not coupled and they are not affected by the presence of particles here, the magnetic force field S_{mr} and S_{mz} can be independently determined at every calculation grid by solving equations (10, 13). The scalar solver of CFD-ACE [21] is used in solving equation (10). At the same time, we use the flow solvers of μThor and CFD-ACE to solve the Navier-Stokes equations and determine the fluid velocity field. The particle velocity at the calculation grids can be obtained by simply solving equations (3), so that the particle trajectories can be consequently determined. The detail of the algorithm is given below:

Step 1: use the flow solvers of μ-Thor and CFD-ACE to solve the fluid velocities at the calculation grid (i, j), i.e. $V_z(i, j)$ and $V_r(i, j)$.

Step 2: use the scalar solver of CFD-ACE to obtain the force field components $S_{mr}(i, j)$ and $S_{mz}(i, j)$.

*Step*3: iterations to solve the particle trajectories and the critical mobilities (an example of determining m_{c1} is used here for better illustration, the particle trajectory therefore starts from the inlet splitter, i.e. $r_p(0)= r_{sin}$. The same procedure can be applied to solve the other critical mobilities.):

a. give an initial guess $m_0 = m$;

b. for k=0, 1, 2 … until convergence;

c. for i=0, 1, 2 … i_{max}-1 and j=0, 1, 2 … j_{max}-1:

- $U_{mz}^{(k)}(i,j) = m_0^{(k)} S_{mz}(i,j)$ and $U_{mr}^{(k)}(i,j) = m_0^{(k)} S_{mr}(i,j)$;
- $r_p^{(k)}(i+1) = r_p^{(k)}(i) + \left[U_{mr}^{(k)}(i) + V_r^{(k)}(i)\right] / \left[U_{mr}^{(k)}(i) + V_z^{(k)}(i)\right] dz(i)$, where $U_{mr}^{(k)}(i)$, $V_r^{(k)}(i)$ and $V_z^{(k)}(i)$ are the interpolated values at the position of [$z(i)$, $r_p^{(k)}(i)$], and $dz(i)$=$z(i$+1)-$z(i)$;
- if $r_p(i) > r_o$ or $r_p(i) < r_i$, $m_0^{(k+1)} = m_0^{(k)} + \delta m$, set i=0 and go to the step c.
- if $r_p^{(k)}(i_{max-1}) - r_{sout}$<error, output the critical mobility m_0 and the corresponding particle trajectory [$z(i)$, $r_p^{(k)}(i)$]. Here r_{sout} is the radius of the outlet splitter as shown in figure 1;
- otherwise, $m_0^{(k+1)} = m_0^{(k)} + \delta m$, set i=0 and go to the step c.

The program is written in the *C* language and is run on a Compaq AlphaStation XP1000. In the calculation of the particle migration velocities, a second order accurate central differential scheme is used. The explicit Euler method is used for the time step. We use very fine grid especially at the channel inlet and outlet (which ensures the time step is small) in order to restrict the numerical error. The convergence can be rapidly achieved due to small number of iterations needed (CPU time is typically in seconds). Solving the flow field and the magnetic force field needs more computational effort; however, these fields are only needed to be solved once. The above calculation starts from

given flow rates to determine the critical mobilities. An optimisation method for the operational flow rates for efficient separation of particles with certain mobilities will be discussed late.

RESULTS AND DISCUSSIONS

The quadrupole magnetic flow sorter used by Hoyos et al. [2] has the geometry of r_o=4.53 mm, r_i=2.38 mm, the inlet splitter radius r_{sin}=3.124 mm and the outlet splitter radius r_{sout}=3.543 mm. The length of the separation channel between the splitters L is 95 mm. The schematic diagram of the device is shown by figure 1. The magnetic flux densities at the outer wall r_o are 0.775 and 1.334 T respectively. The magnets' bore radii are 4.85 and 4.82 mm, with length of 76.2 mm i.e. L_m=76.2 mm. Under the operation conditions, the ratio of the fractional flow rates is kept constant, i.e. Q_a^{out}/Q=0.2 and Q_a^{in}/Q=0.1. In the calculations, Hoyos et al. [2] adopted the theory of Williams et al. [4] which ignores the fringing force field near the splitters, so that the Kelvin force acting on the particle was only considered in the r direction within the channel region covered by the length of magnet. In doing so, the effect of the flow development regions at the splitters was assumed to be negligibly small because the flow is fully-developed within the force field. Therefore, in their calculations, the effective separation channel length is 76.2 mm while it is actually 95.0 mm. In this paper, we focus on the effects of the flow development region and the fringing magnet force field, we assume the splitters are very thin and have the similar magnetic permeability to the surrounding liquid. Although the thickness of the splitters may play a role, it is believed to be small for creeping flows especially when the magnet length is restricted within the fully-developed flow region because the streamlines there remain the same regardless of possible splitter thickness and $\nabla|B|$ is close to zero at the vicinity of the splitters. However, if the length of magnet covers whole separation channel, the splitter thickness will have bigger impact on the particle trajectories. Geometric imperfections may have more significant influence, which has been discussed by Williams et al. [6].

First, the streamlines of the flow field and the contour of the magnitude of $\boldsymbol{B}$ at the separation channel inlet and outlet are shown in figures 2 and 3. It is clear that the streamlines are not parallel in the regions where the flow is not fully-developed, and the force field in the axial direction does exist i.e. $\partial B / \partial z \neq 0$. Therefore, it may not be appropriate to ignore the effects of the flow development regions and the fringing force field. As L.R. Moore and P.S. Williams pointed out in a private discussion, the fringing magnet field is strongest close to the planes of symmetry of the pole pieces. This is caused by the end surface of the quadrupole magnet, a more thorough examination may need to consider this 3-dimensional effect. Here, we only consider the worst case where the fringing field is strongest and examine the effect.

Figure 4 shows *ISS* and *OSS* stream-lines and the particle trajectories. The flow rate Q=60 ml/min and B_0=1.334 T. Here, the critical mobilities m_0, m_1 and m_2 are 3.98×10^{-4}, 8.09×10^{-4} and 21.38×10^{-4} mm^3/TAs respectively. The corresponding trajectories are shown by dash-dot lines. In present approach, these mobilities are obtained numerically which are also consistent with equations (16-18). If the particles with mobility m_m=12.0×10^{-4} mm^3/TAs ($m_1 < m_m < m_2$) enter the separation channel through the inlet *a*, they will be collected at the outlet *b* without sticking to the wall regardless of their initial entry positions. The possible trajectories of these particles will be between the two solid lines marked by m_m. Figure 5 also confirms that any particle with mobility, m_m, satisfying $m_1 < m_m < m_2$, will be totally separated without sticking to the wall. The flow rate Q is 10 ml/min and B_0 is 0.775 T in this figure. Therefore, the most important factor for optimisation of operational flow rates is to design the values of m_1 and m_2 to ensure the mobilities of the particles to be separated fall in-between.

Suppose there are two type of particles with mobilities m_{m1}= 1.0×10^{-4} mm^3/TAs and m_{m2}=3.0×10^{-4} mm^3/TAs, can they be efficiently separated under current operation conditions with Q=10 ml/min and B_0 =0.775 T? First, we solve the critical mobilities: m_0=1.91×10^{-4} mm^3/TAs,

m_1=3.91×10^{-4} mm^3/TAs and m_2=10.58×10^{-4} mm^3/TAs. The corresponding particle trajectories are shown in figure 6. Because $m_{m1} < m_0$ and $m_{m2} > m_0$, these particles can be separated. However, since $m_{m2} < m_1$, the particles with mobility of m_{m2} can only be separated if their initial position is close to the inlet splitter (the lower solid line marked by m_{m2} shows the dividing entry position below which the particles cannot move across to the outlet *b*). The particles with mobility m_{m1} cannot move across even initially starting at the inlet splitter as shown by the solid line marked with m_{m1}. Therefore, if the particles are evenly distributed at the inlet *a*, the separation ratio in this case is not good because the operation flow rates are not optimised.

However, the particles with large mobility m_m=12.0×10^{-4} mm^3/TAs which is larger than m_2, will all move across the *OSS* streamline but may stick to the separation channel wall depending on the initial entry positions. As shown in figure 7, the particles move in the separation channel between the upper solid line marked by m_m and the inlet splitter will all hit the channel wall at the outlet *b*. All these figures confirm the importance of the critical mobilities which depend on the flow rates if the magnet flux density is given. We need to ensure the less mobile particles with mobilities smaller than m_0, and higher mobile particles with mobilities between m_1 and m_2, at the same time, the critical mobilities have to satisfy $m_1 < m_2$.

Table 1 shows the critical mobilities calculated from the present theory and the theory of Williams et al. [4]. The relatively small difference in critical mobilities can be caused by the effect of the flow development regions and the fringing magnetic force field at the separation channel inlet and outlet. As shown in tables 1, very close m_2 is predicted by both theories, but Williams et al. have lower values for m_0 and m_1. At a low flow rate, critical mobilities are small, thus the separation rate will mainly be proportional to $m_2 - m_1$. Therefore, Williams et al. may overestimate the separation rate. At a large flow rate, critical mobilities are larger, so that the mobility distribution

is shifted to the other end, thus the separation rate mainly depends on the values of m_0 and $m_1 - m_0$. In this case, Williams et al. also overestimates the separation rate. However, both predictions for m_1 are within a deviation less than 10%, the resulting difference in separation rate prediction will be smaller. Here, we need to emphasize that the variation of fringing magnetic field around circumference of the annular channel is ignored and the strongest fringing field is used in this calculation. Therefore the discrepancy between current approach and the theory of Williams et al. may be smaller in weaker fringing field region. A 3D simulation is needed to accurately assess the impact of angular variation of fringing magnetic field.

Because the theory of Williams et al. [4] can have simplified analytical solutions for the flow field and the magnetic force field, the computational effort for the optimisation of the operation conditions is much less than the present approach. In above study, the magnet length was designed to restrict the force field to be within the fully-developed flow region in order to avoid the effect of the flow development regions. Here, we propose to extend the length of magnet to cover whole separation channel so that L equals to L_m in figure 1. The discrepancy between the present theory and the theory of Williams et al. [4] is to be examined below.

The fringing force field is shown in figure 8, compared to figure 3, the axial variations are greater at the inlet and outlet channel walls, so that the particles will experience a rapid deviation from the corresponding streamlines near the wall region, which is confirmed by the particle trajectories shown in figure 9. The comparison of the critical mobilities among the predictions of the present theory, the theory of Williams et al. and the present theory but ignoring the fringing force field (denoted by Present, PSW and Non-fringing respectively) is shown in table 2. We can see that ignoring the fringing force fields but considering the effect of the flow development regions will improve the predictions compared to the simpler theory of Williams et al. If we compare the critical mobilities predicted by the present theory for two different channel length L= 95 and 76.2 mm with the theoretical predictions of Williams et al. where the effective channel length is assumed 76.2 mm

in both cases, we find that restricting the magnet length to the fully-developed flow region does not have any improvement of the theoretical predictions of Williams et al. Therefore, the effect of flow development regions cannot be avoided by doing so.

CONCLUSIONS

The effect of flow development regions and fringing magnetic field has been investigated, where only the strongest fringing field on the plane of symmetry passing through the centre-line of a pole piece is considered. Overall, using the theory of Williams et al. [4] to optimise the operation conditions is sufficient for most cases. The advantage of this theory is that no iterations are needed so that the computing time is small. The present approach needs to solve flow fields and force fields first, and then iterations are needed to determine the critical mobilities, so that it requires more computational effort. If the present approach is used to optimise the operation flow rates, we can use the results of the theory of Williams et al. as initial inputs in order to reduce computing time significantly and achieve more accurate predictions.

ACKNOWLEDGEMENT

This work is financially supported by UK Medical Research Council under grant reference 57719. The authors are very grateful to M. Zborowski, P. S. Williams, and L. R. Moore for their insightful and helpful comments.

REFERENCES

[1] M. Zborowski, L. Sun, L.R. Moore, P.S. Williams, J.J. Chalmers, J. Magnetism Magn. Mater. 194 (1999) 224.

[2] M. Hoyos, L.R. Moore, K.E. McCloskey, S. Margel, M. Zuberi, J.J. Chalmers, M. Zborowski, J. Chromatogr. A 903 (2000) 99.

[3] M. Nakamura, K. Decker, J. Chosy, K. Comella, K. Melnik, L. Moore, L.C. Lasky, M. Zborowski, J.J. Chalmers, Biotechnol. Prog. 17 (2001) 1145.

[4] P.S. Williams, M. Zborowski, J.J. Chalmers, Anal. Chem. 71 (1999) 3799.

[5] M. Hoyos, K.E. McCloskey, L.R. Moore, M. Nakamura, B.J. Bolwell, J.J. Chalmers, M. Zborowski, Sep. Sci. Technol. 37 (2002) 745.

[6] P.S. Williams, L.R. Moore, J.J. Chalmers, M. Zborowski, Anal. Chem. 75 (2003) 1365.

[7] C.B. Fuh, M.N. Myers, J.C. Giddings, Anal. Chem. 64 (1992) 3125.

[8] P.S. Williams, Sep. Sci. Technol. 29 (1994) 11.

[9] P.S. Williams, S. Levin, T. Lenczycki, J.C. Giddings, Ind. Eng. Chem. Res. 31 (1992) 2172.

[10] Y. Jiang, A. Kummerow, M. Hansen, J. Microcolumn Sep. 9 (1997) 261.

[11] S. Gupta, P.M. Ligrani, J.C. Giddings, Sep. Sci. Technol. 32 (1997) 1629.

[12] P.M. Ligrani, S. Gupta, J.C. Giddings, Int. J. Heat Mass Transfer 41 (1998) 1667.

[13] S. Gupta, P.M. Ligrani, J.C. Giddings, Int. J. Heat Mass Transfer 42 (1999) 1023.

[14] Y. Zhang, D.R. Emerson, J.M. Reese, J. Chromatogr. A. 1010 (2003) 87.

[15] S.R. Springston, M.N. Myers, J.C. Giddings, Anal. Chem. 59 (1987) 344.

[16] L.S. Fan, C. Zhu, Principles of gas-solid flows, Cambridge University Press, Cambridge, 1998.

[17] R. Clift, J.R. Grace, M.E. Weber, Bubbles, drops, and particles, Academic Press, London, 1978.

[18] R.J. Hunter, Foundations of Colloid Science, 2nd ed,; Oxford Press, New York, 2001.

[19] C. Crowe, M. Sommerfield, Y. Tsuji, Multiphase flows with droplets and particles, CRC Press, London, 1998.

[20] H.E. Knoepfel, Magnetic fields: a comprehensive theoretical treatise for practical use, John Willey & Sons, New York, 1999.

[21] CFD Research Corporation, Cummings Research Park, 215 Wynn Drive, Huntsville, AL 35805, USA.

[22] J.H. Ferziger, M. Perić, Computational methods for fluid dynamics, 3rd ed., Springer, Berlin, 2002.

FIGURE CAPTIONS

Figure 1. Schematic diagram of an annular quadrupole magnetic flow sorter.

Figure 2. Streamlines at the separation channel inlet and outlet, Q=60 ml/min.

Figure 3. The fringing field of the magnitude of $\boldsymbol{B}$ at the separation channel inlet and outlet, B_0=1.334 T. Here, variation of the fringing field around the circumference of the annular channel is ignored.

Figure 4. Particle trajectories and *ISS*, *OSS* stream-lines in the separation channel, where the total flow Q=60 ml/min, the magnet flux density B_0=1.334 T. The magnetophoretic mobilities are: m_0= 3.98×10^{-4}, m_1 = 8.09×10^{-4}, m_2= 21.38×10^{-4}, and m_m= 12.0×10^{-4} mm^3/TAs respectively.

Figure 5. Particle trajectories and *ISS*, *OSS* stream-lines in the separation channel, where the total flow Q=10 ml/min, the magnet flux density B_0=0.775 T. The magnetophoretic mobilities are: m_0= 1.91×10^{-4}, m_1 = 3.91×10^{-4}, m_2= 10.58×10^{-4} and m_m= 7.0×10^{-4} mm^3/TAs respectively.

Figure 6. Particle trajectories and *ISS*, *OSS* stream-lines in the separation channel, where the total flow Q=10 ml/min, the magnet flux density B_0=0.775 T. The magnetophoretic mobilities are: m_0= 1.91×10^{-4}, m_1 = 3.91×10^{-4}, m_2= 10.58×10^{-4}, m_{m1}=1.0×10^{-4} and m_{m2}=3.0×10^{-4} mm^3/TAs respectively.

Figure 7. Particle trajectories and *ISS*, *OSS* stream-lines in the separation channel, where the total flow Q=10 ml/min, the magnet flux density B_0=0.775 T. The magnetophoretic mobilities are: m_0= 1.91×10^{-4}, m_1 = 3.91×10^{-4}, m_2= 10.58×10^{-4} and m_m=12.0×10^{-4} mm^3/TAs respectively.

Figure 8. The fringing force field at the splitters, B_0=1.334 T. Here, variation of the fringing field around the circumference of the annular channel is ignored.

Figure 9. Particle trajectories and *ISS*, *OSS* stream-lines in the separation channel, where the total flow Q=60 ml/min, the magnet flux density B_0=1.334 T. The magnetophoretic mobilities are: m_0 = 3.94×10^{-4}, m_1 = 8.15×10^{-4}, m_2 = 21.50×10^{-4}, and m_m =15.0×10^{-4} mm^3/TAs respectively.

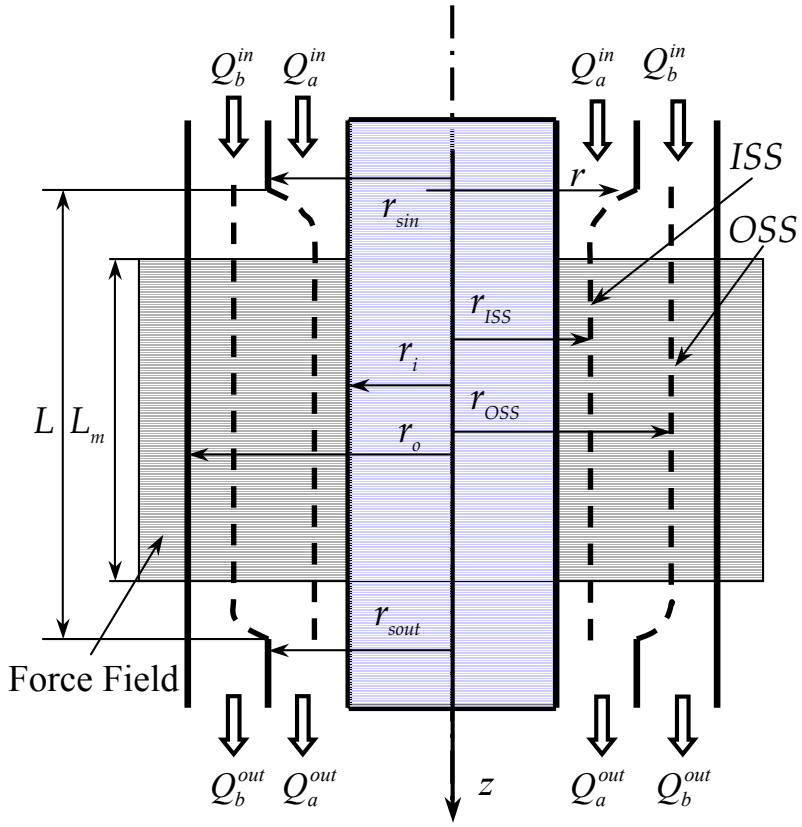

Figure 1. Schematic diagram of an annular quadrupole magnetic flow sorter.

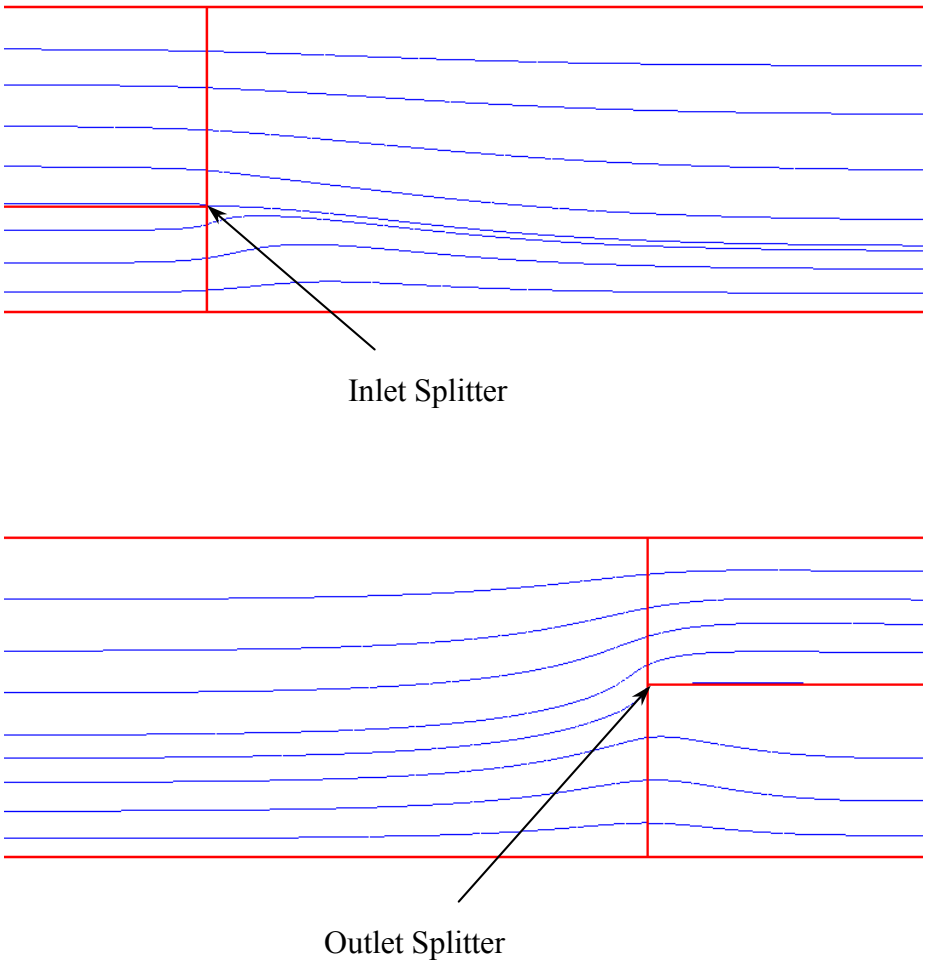

Figure 2. Streamlines at the separation channel inlet and outlet, Q=60 ml/min.

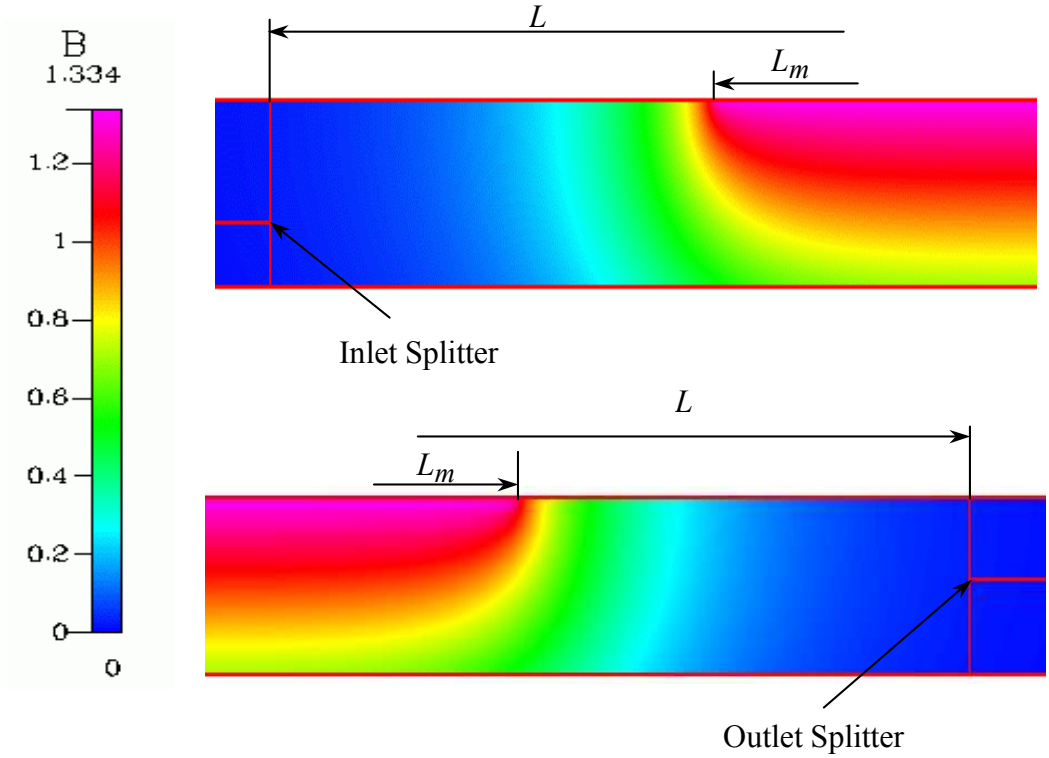

Figure 3. The fringing field of the magnitude of ***B*** at the separation channel inlet and outlet, B_0=1.334 T. Here, variation of the fringing field around the circumference of the annular channel is ignored.

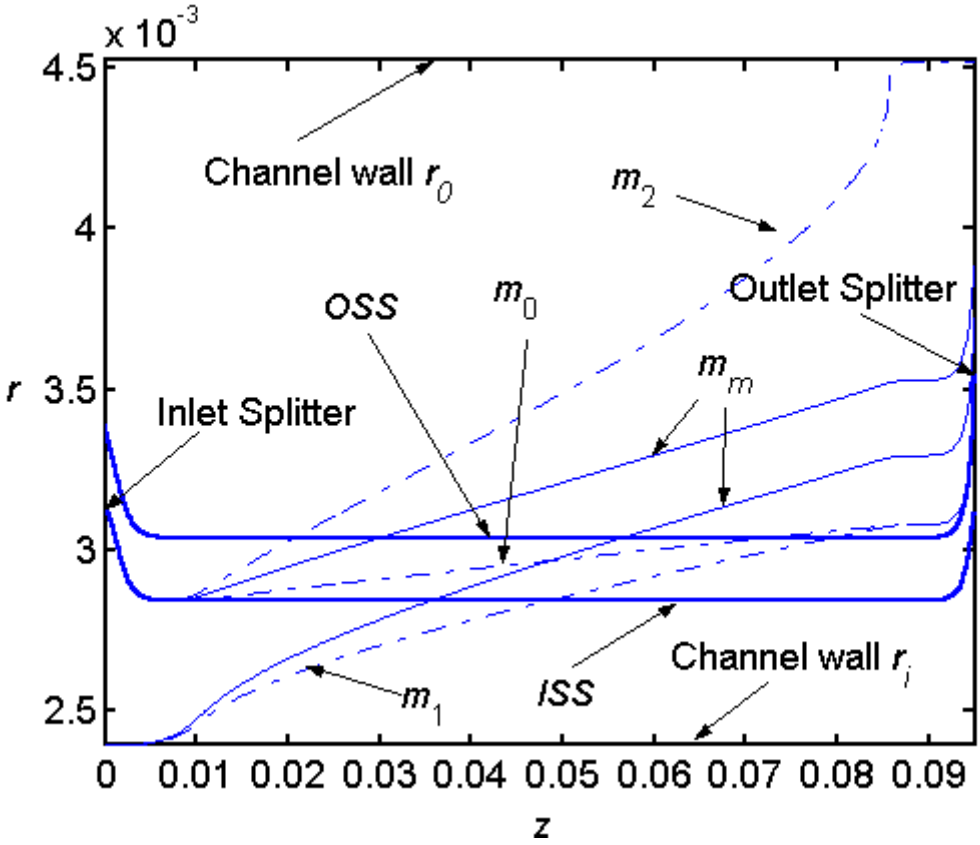

Figure 4. Particle trajectories and *ISS*, *OSS* stream-lines in the separation channel, where the total flow Q=60 ml/min, the magnet flux density B_0=1.334 T. The magnetophoretic mobilities are: m_0 = 3.98×10^{-4}, m_1 = 8.09×10^{-4}, m_2 = 21.38×10^{-4}, and m_m = 12.0×10^{-4} mm^3/TAs respectively.

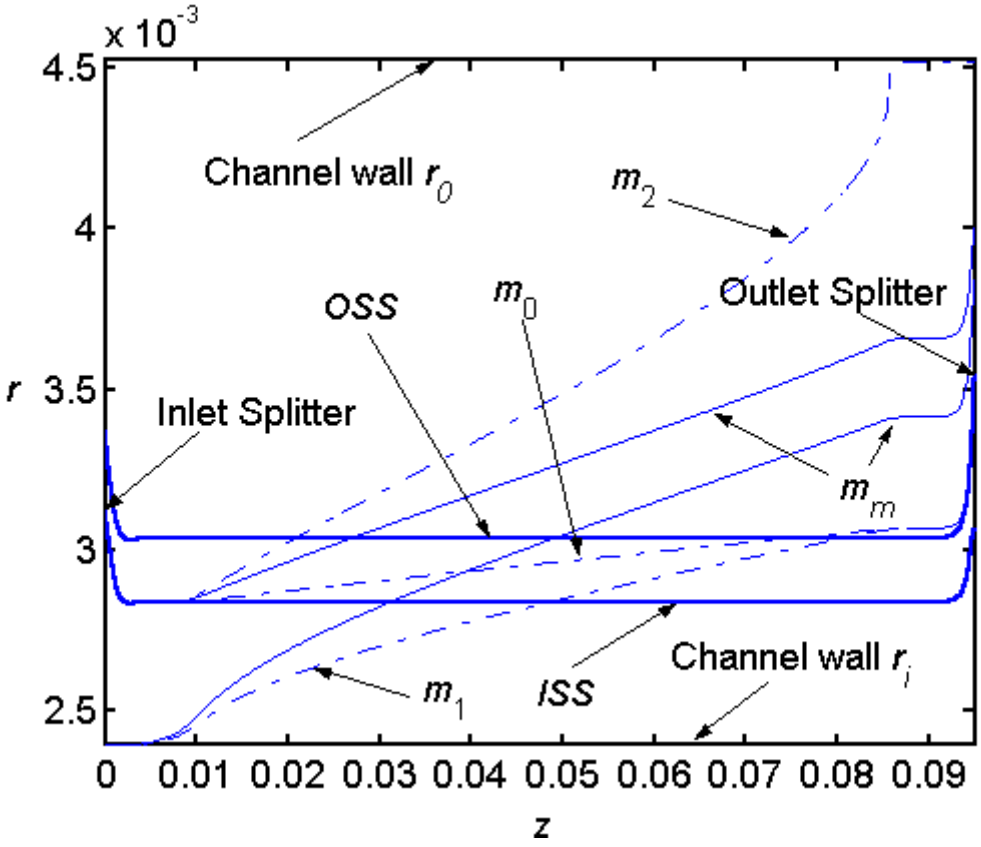

Figure 5. Particle trajectories and *ISS*, *OSS* stream-lines in the separation channel, where the total flow Q=10 ml/min, the magnet flux density B_0=0.775 T. The magnetophoretic mobilities are: m_0 = 1.91×10^{-4}, m_1 = 3.91×10^{-4}, m_2 = 10.58×10^{-4} and m_m = 7.0×10^{-4} mm^3/TAs respectively.

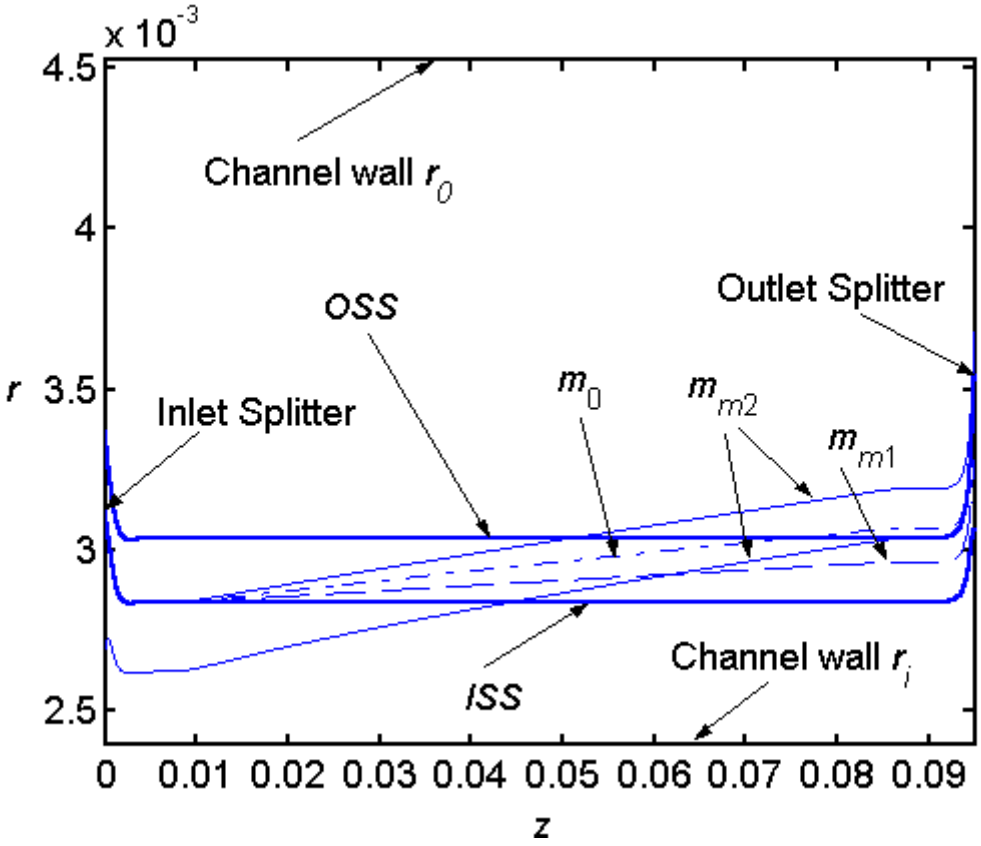

Figure 6. Particle trajectories and *ISS*, *OSS* stream-lines in the separation channel, where the total flow Q=10 ml/min, the magnet flux density B_0=0.775 T. The magnetophoretic mobilities are: m_0= 1.91×10^{-4}, m_1 = 3.91×10^{-4}, m_2= 10.58×10^{-4}, m_{m1}=1.0×10^{-4} and m_{m2}=3.0×10^{-4} mm^3/TAs respectively.

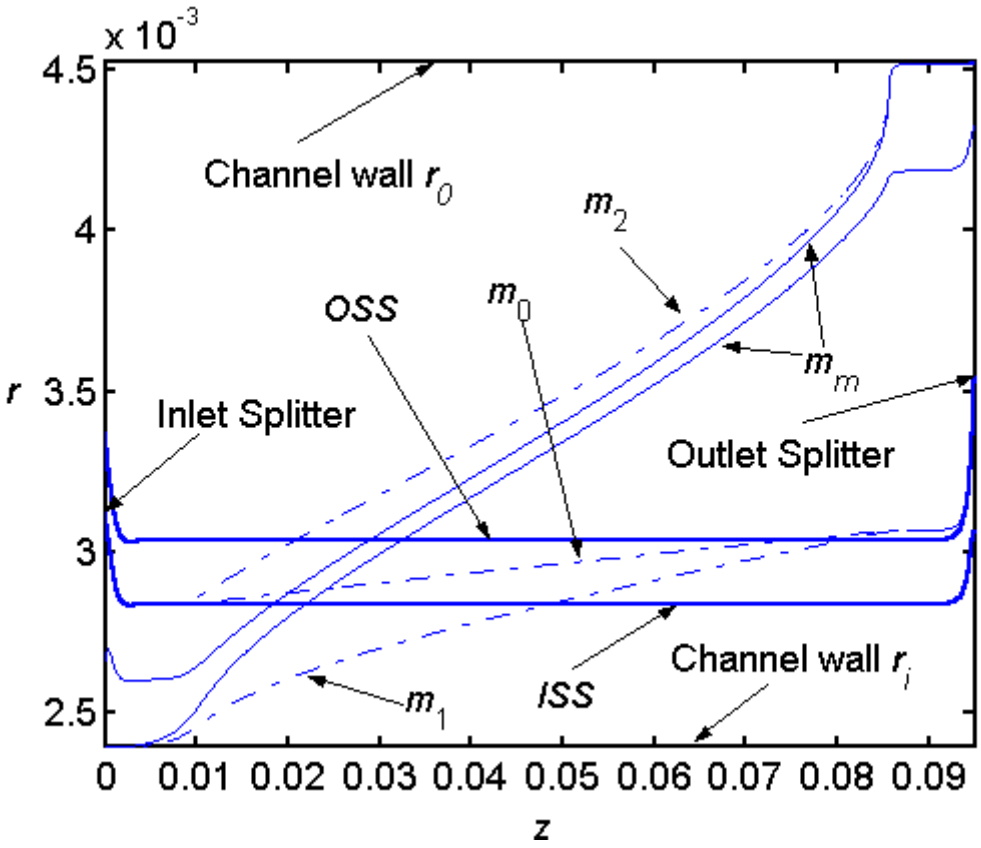

Figure 7. Particle trajectories and *ISS*, *OSS* stream-lines in the separation channel, where the total flow Q=10 ml/min, the magnet flux density B_0=0.775 T. The magnetophoretic mobilities are: m_0 = 1.91×10^{-4}, m_1 = 3.91×10^{-4}, m_2 = 10.58×10^{-4} and m_m =12.0×10^{-4} mm^3/TAs respectively.

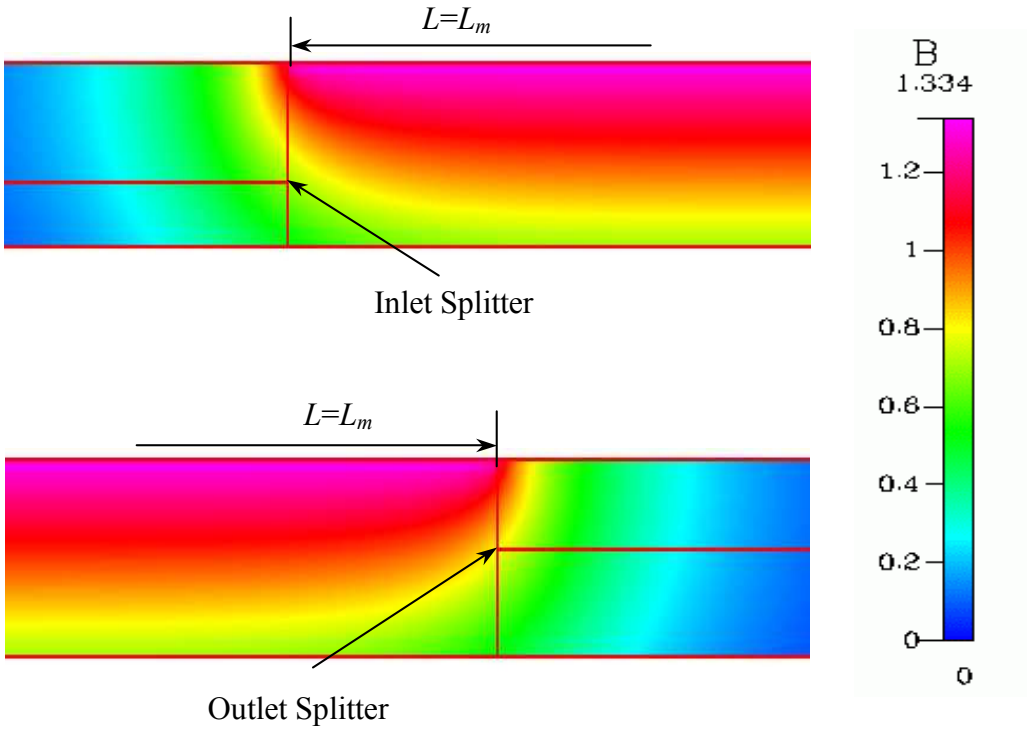

Figure 8. The fringing force field at the splitters, B_0=1.334 T. Here, variation of the fringing field around the circumference of the annular channel is ignored.

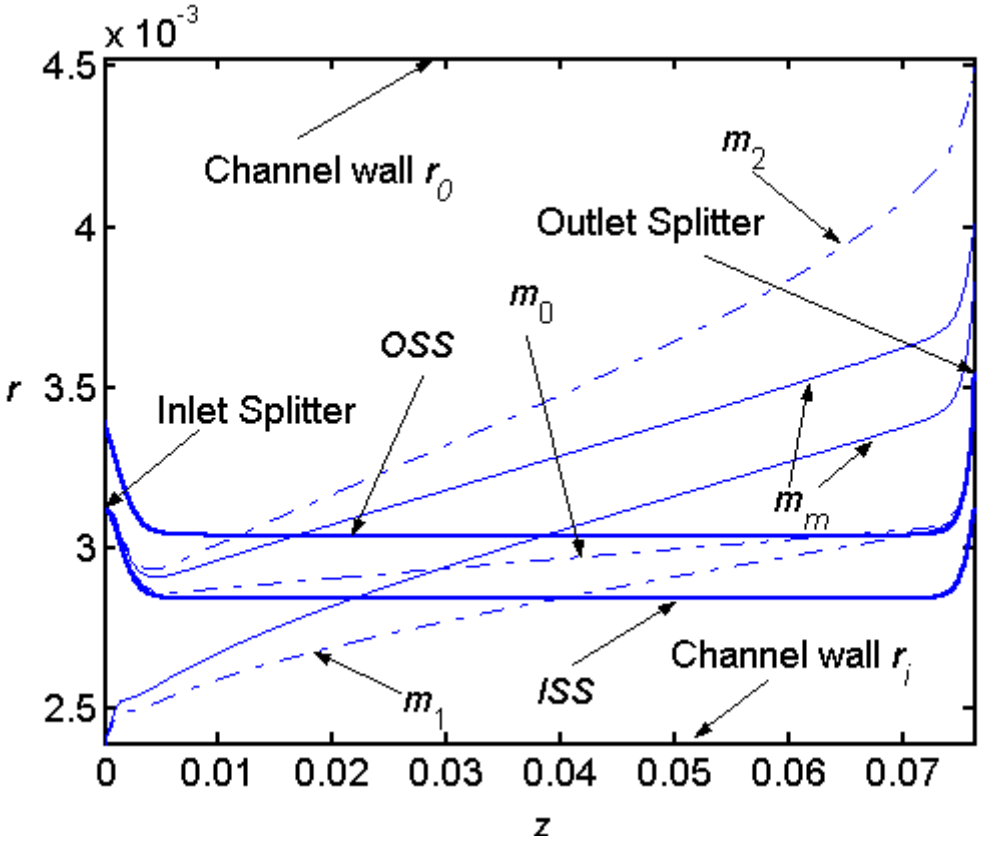

Figure 9. Particle trajectories and *ISS*, *OSS* stream-lines in the separation channel, where the total flow Q=60 ml/min, the magnet flux density B_0=1.334 T. The magnetophoretic mobilities are: m_0 = 3.94×10^{-4}, m_1 = 8.15×10^{-4}, m_2 = 21.50×10^{-4}, and m_m =15.0×10^{-4} mm^3/TAs respectively.

Table 1. Calculated critical magnetophoretic mobilities under different flow rates and magnet flux densities. B_0=1.334 T for the values in the grey columns and B_0=0.755 T for the values in the white columns.

Q (ml/min)	$m_0 \cdot 10^4$ (mm^3/TAs)				$m_1 \cdot 10^4$ (mm^3/TAs)				$m_2 \cdot 10^4$ (mm^3/TAs)			
	PSW[1]		Present[2]		PSW[1]		Present[2]		PSW[1]		Present[2]	
60	3.29	9.75	3.98	11.80	7.51	22.26	8.09	23.97	21.99	65.16	21.38	63.36
30	1.66	4.91	1.96	5.81	3.76	11.13	4.01	11.87	11.01	32.61	10.70	31.73
10	0.56	1.66	0.65	1.91	1.25	3.72	1.32	3.91	3.67	10.88	3.57	10.58
5	0.28	0.83	0.32	0.95	0.63	1.86	0.66	1.95	1.84	5.44	1.79	5.29

1. The predictions of the theory of Williams et al.[4]
2. The predictions of the present theory.

Table 2. Calculated critical magnetophoretic mobilities under different flow rates with B_0=1.334 T and L=L_m.

Q (ml/min)	$m_0 \cdot 10^4$ (mm^3/TAs)			$m_1 \cdot 10^4$ (mm^3/TAs)			$m_2 \cdot 10^4$ (mm^3/TAs)		
	PSW[1]	Present[2]	Non-fringing[3]	PSW[1]	Present[2]	Non-fringing[3]	PSW[1]	Present[2]	Non-fringing[3]
60	3.29	3.94	3.93	7.51	8.15	8.10	21.99	21.50	21.89
30	1.66	1.95	1.94	3.76	4.04	4.02	11.01	10.78	10.98
10	0.56	0.64	0.64	1.25	1.33	1.33	3.67	3.60	3.67
5	0.28	0.32	0.32	0.63	0.66	0.66	1.84	1.80	1.84

1. The predictions of the theory of Williams et al.[4]
2. The predictions of the present theory.
3. The predictions are obtained by ignoring the fringing force field, i.e. the force field is described by equation (22).